Resting-State EEG Microstates Across a Dimensional Spectrum of Autistic Traits: From Typical Development to Diagnosed ASD

Title:

Resting-State EEG Microstates Across a Dimensional Spectrum of Autistic Traits: From Typical Development to Diagnosed ASD

Authors:

Tania Karina Garcia Vite [1,2]

Achilleas Pavlou [3]

Christina Pari [2]

Tom Foulsham [1]

Nicholas Cooper [1]

Affiliations:

1 University of Essex, Wivenhoe Park, Colchester CO4 3SQ, United Kingdom

2 CYENS Centre of Excellence, Lellou Demetriades, Plateia Dimarchou 1, Nicosia 1016

3 University of Nicosia, 46 Makedonitissas Avenue, CY-2417

Corresponding author:

Tania Karina Garcia Vite

t.garcia@cyens.org.cy

Present Address:

CYENS Centre of Excellence, Lellou Demetriades, Plateia Dimarchou 1, Nicosia 1016

Abstract

Autism spectrum disorder (ASD) has been linked to atypical large-scale brain dynamics, but it is unclear how these alterations extend across the broader autism phenotype. We applied a seven-class resting-state EEG microstate model (A–G) to adults with clinical ASD and to typically developing adults with high (TD-High) and low (TD-Low) autistic traits, quantified with the Autism-Spectrum Quotient. We compared temporal parameters, spatial coverage, explained variance, and both observed and chance-corrected transition probabilities.

Across all microstates, the ASD group showed a globally more fragmented regime than both TD groups, with markedly shorter but more frequent microstate episodes and reduced duration variability. By contrast, TD-High and TD-Low were similar on these global indices. At the network level, Microstate C showed reduced explained variance and coverage in ASD relative to both TD groups. In Microstates E and G, explained variance and coverage increased from TD-Low to TD-High to ASD, with TD-High consistently occupying an intermediate position. Mean GFP and GFP variability for Microstate E were also elevated in ASD relative to both TD groups.

Transition analyses revealed reduced short-range transitions within an early A–C ensemble and increased transitions from these states into other microstates in ASD, with TD-High again showing an attenuated, intermediate pattern. Chance-corrected transitions confirmed that sensory/self-related routes occurred less often than expected, whereas routes from these states into other microstates were over-expressed.

These findings support a dimensional account in which EEG microstates index autism-related network organisation across clinical and subclinical ranges.

Graphical abstract

Resting-State EEG Microstates Across a Dimensional Spectrum of Autistic Traits

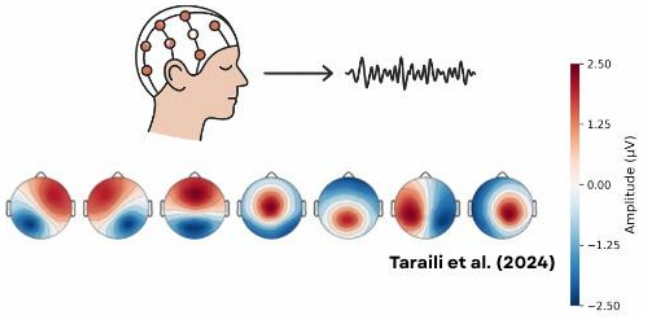

BROADER AUTISM PHENOTYPPE

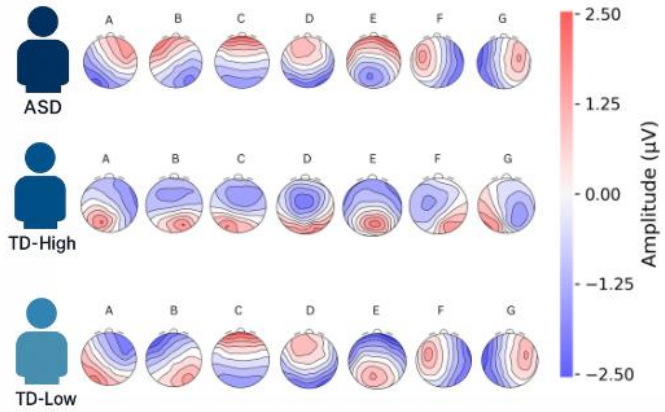

Findings support the dimensional model of autistic traits and highlight EEG microstates as promising tools for tracking spontaneous and task-driven neural alterations across the autism spectrum.

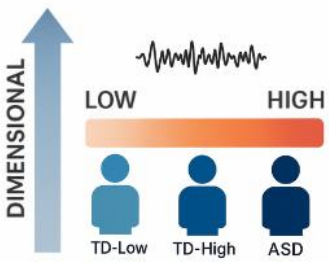

Keywords

EEG Microstates, Autism Spectrum Disorder, Broader Autism Phenotype, Salience Network, Default Mode Network, Neural Dynamics

1. Introduction

Autism spectrum disorder (ASD) is increasingly characterised as a condition of altered large-scale brain dynamics, yet how these alterations extend across the broader autism phenotype (BAP) remains under-specified. EEG microstates—brief, quasi-stable scalp topographies tiling spontaneous activity on the order of tens of milliseconds—provide a window onto rapid reconfigurations of large-scale functional states that complements slower hemodynamic measures (Lehmann et al., 2009; Khanna et al., 2015; Michel & Koenig, 2018; Van de Ville et al., 2010).

Beyond the traditional four-class solution, source-informed seven-class taxonomies (A–G) improve functional interpretability by aligning microstate maps with canonical resting-state networks (RSNs). Building on Custo et al. (2017) and the recent synthesis by Tarailis and colleagues, we adopt a taxonomy in which Microstate A is linked to audio-visual processing and arousal, Microstate B to self-related visual imagery and autobiographical memory, Microstate C to personally significant and self-referential mentation, Microstate D to executive/attentional control, Microstate E to interoceptive–emotional and salience processing, Microstate F to default mode network (DMN) and Theory-of-Mind (ToM)–related mentation, and Microstate G to somatosensory/sensorimotor processing. This functionally grounded A–G framework allows a more fine-grained mapping between microstate dynamics and large-scale network organisation than four-class schemes.

Several studies have reported atypical microstate profiles in ASD, most often involving visually biased Microstate B and DMN-related Microstate C. Across individual reports, ASD has been associated with increased duration and coverage of Microstate B and reduced presence of Microstate C, alongside more variable findings for attention- and sensorimotor-related states (e.g., Das et al., 2022; Takarae et al., 2022; Kalburgi et al., 2023). A recent meta-analysis confirmed that, at the group level, Microstate B coverage and duration tend to be greater in ASD, whereas Microstate C occurrence is reduced, but also showed substantial heterogeneity across studies and highlighted age as a major moderator of effect size and direction. These inconsistencies likely reflect differences in age range, symptom severity, analytic pipelines, and microstate taxonomies.

Much less is known about how these microstate alterations extend into the non-clinical range. Autistic traits are continuously distributed in the general population and can be quantified with the Autism-Spectrum Quotient (AQ; Baron-Cohen et al., 2001). However, clinical ASD and

high-trait typical individuals are rarely examined within a single, harmonised microstate framework. As a result, it remains unclear whether typically developing individuals with high autistic traits (TD-High) show microstate profiles intermediate between clinical ASD and low-trait typical adults (TD-Low), or whether clinical ASD reflects qualitatively distinct network dynamics rather than an extension of Broad Autism Phenotype (BAP) related variation (Hull et al., 2017).

In addition to standard temporal parameters (mean duration, occurrence, coverage, explained variance), transition structure provides a complementary window on large-scale dynamics. First-order transition matrices quantify how often the brain moves from one microstate to another, while chance-corrected deviations (ΔTM; observed minus expected transitions given each state's base rate) disentangle differences in state occupancy from differences in preferential routing between networks. Applying both organisational transition probabilities (OrgTM) and ΔTM can therefore reveal whether group effects arise from spending more time in particular states, from atypical patterns of switching between them, or both.

Aims and research questions

Guided by RSN-based seven-class microstate taxonomies and dimensional accounts of the BAP, this study had three main aims:

1. **Temporal dynamics across seven microstates.** To characterise group differences in resting-state microstate temporal dynamics (A–G) in adults with ASD, TD-High, and TD-Low, focusing on mean duration, occurrence rate, coverage, GFP-based strength, and explained variance.

2. **Transition structure.** To quantify group differences in microstate transition dynamics, analysing both raw organisational transition probabilities (OrgTM) and chance-corrected deviations (ΔTM = OrgTM − expected) in order to separate effects driven by state occupancy from differences in preferential routing between microstates.

3. **Positioning within the broader autism phenotype.** To situate any observed differences within a dimensional BAP framework by testing whether TD-High participants show intermediate microstate profiles between ASD and TD-Low, and by exploring associations between AQ scores and key microstate parameters across the combined sample.

By combining an open clinical ASD dataset with newly collected AQ-stratified typical cohorts, processed under a harmonised preprocessing and microstate pipeline, we aim to provide an integrated picture of how large-scale electrophysiological dynamics vary from low-trait typical adults, through high-trait individuals, to clinically diagnosed ASD.

2. Methods

2.1. Demographics & Ethics

EEG microstate analysis was conducted on three groups: individuals with clinical ASD (Milne, 2021), a high-AQ typical group, and a low-AQ typical group. The publicly available ASD dataset comprised of 28 adults (12 female; M = 44.34 ± 13.31 years; range = 18–67) with clinician-confirmed diagnoses under DSM-IV, DSM-V, or ICD-10 criteria, as described by Dickinson, Jeste, & Milne (2022). The clinical ASD group had a mean Social Responsiveness Scale (SRS) score of 67.71 (SD = 10.01).

For the typically developing cohort, 5000 recruitment emails were distributed through the university mailing list, SONA, and word of mouth. Of 291 respondents who completed the Autism-Spectrum Quotient (AQ; Baron-Cohen et al., 2001), high- and low-AQ groups were defined as ≥1 SD above and ≤1 SD below the sample mean (M = 18, SD = 6), yielding cut-offs of ≥24 (TD-High) and ≤13 (TD-Low). Forty volunteers were invited for EEG recording. The TD-High group (n = 21; 10 female, 11 male; M age = 22.76 ± 4.76 years, range 18–36) and the TD-Low group (n = 19; 13 female, 6 male; M age = 22.42 ± 4.09 years, range 17–31) reflect the upper and lower extremes of typical trait variation, not clinical ASD (AQ ≥ 32 indicates clinically significant levels of autistic traits). All procedures were approved by the University of Essex Ethics Committee (NC1612), and written informed consent was obtained.

2.2. Preprocessing and Software Environment

All analyses were performed in MATLAB (R2024b) using EEGLAB (2024.2) and the MICROSTATELAB plugin (Poulsen et al., 2018). Preprocessing followed the standardized pipeline of Dickinson et al. (2022) to ensure consistency across datasets. Continuous EEG was filtered (1–40 Hz), resampled to 512 Hz, visually inspected for artifacts, re-referenced to the average, and interpolated to the standard 25-channel 10-20 montage. Independent Component Analysis (ICA) was applied for artifact rejection using ICLabel with a ≥ 75% confidence threshold, and Artifact Subspace Reconstruction (ASR; k = 20) removed transient high-amplitude noise. The first 120s of artifact-free data were retained for microstate extraction, ensure comparability between the TD and clinical ASD dataset.

2.3. Microstate Analysis

2.3.1. Microstate Clustering Procedure

Microstate segmentation followed the k-means approach of Kalburgi et al. (2023). Clustering was restricted to Global Field Power (GFP) peaks to emphasize high signal-to-noise time points, with polarity ignored (Khanna et al., 2015). EEG maps were normalized before clustering to

prevent amplitude bias. Cluster solutions ranging from 4 to 7 microstates were explored, and the algorithm was restarted 20 times to ensure stable convergence.

2.3.2. Back-Fitting and Temporal Parameter Extraction

Prototypical microstate maps were back-fitted to continuous EEG, restricted to GFP peaks, using a smoothness parameter $\lambda = 0.3$ and a 30 ms temporal smoothing window (Michel & Koenig, 2018). For each participant, standard temporal metrics—mean duration, occurrence, and coverage—and spatial transition measures were computed. Duration reflects network stability, occurrence captures engagement frequency, and coverage quantifies the proportion of time each network dominates (Khanna et al., 2015; Michel & Koenig, 2018). Transition matrices were computed both as observed transitions (OrgTM) and as chance-corrected deviations ($\Delta TM = OrgTM - ExpTM$), representing preferential or disrupted network switching.

2.3.3. Template Sorting and Group-Level Averaging

Microstate classes were sorted using the seven-map template of Custo et al. (2017), consistent with recent ASD research (Das et al., 2024; Ran et al., 2023; Portnova & Martynova, 2023). Group-level mean maps were computed for each cohort (ASD, TD-High, TD-Low) and re-sorted using the same template. A grand-average map across all participants was generated for visualization and cross-group alignment.

2.4. Statistical Analysis

We assessed group-level differences in EEG microstate dynamics across the three groups (ASD, TD-High, TD-Low) using a hierarchical analysis framework consisting of omnibus group tests, gated post-hoc comparisons, and correction for multiple comparisons using the Benjamini–Hochberg false discovery rate (FDR).

Microstate Variables

The following EEG microstate metrics were extracted and analyzed:

- **Temporal metrics** (per microstate class A–G):
    - *Mean duration*, *occurrence rate* (Hz), and *duration standard deviation*
    - *Across-class averages* for duration and occurrence (MeanDurationAll, MeanOccurrenceAll)
- **Coverage metrics**:
    - *Coverage* (i.e., percent time occupied) for each microstate class

- **Strength/amplitude metrics**:
    - *Mean global field power (GFP)* and *GFP standard deviation* per microstate class
- **Explained variance metrics**:
    - *Variance explained* by each microstate class (IndExpVar_X) and *total explained variance* across all classes (TotalExpVar)
- **Transition dynamics**:
    - *Observed transition probabilities* (OrgTM; e.g., A→B) and
    - *Chance-adjusted transition probabilities* (DeltaTM), derived by subtracting expected transition frequencies from observed values
    - A total of 42 directed transitions were evaluated in each matrix

Group Comparisons

For each scalar variable, we first conducted an omnibus test across the three groups. Normality was assessed with the Shapiro–Wilk test, and homogeneity of variance with a median-centered Levene's test. When both assumptions were met, a one-way ANOVA was used and η^2 was reported as the effect size. If assumptions were violated, a Kruskal–Wallis test was applied, and ε^2 was reported.

Post-hoc pairwise group comparisons (ASD vs TD-High, ASD vs TD-Low, TD-High vs TD-Low) were conducted only when the corresponding omnibus test was significant at $p < .05$. Welch's *t*-tests were used for parametric data and Dunn's tests (with tie correction) for non-parametric data. Effect sizes were estimated using Cliff's delta, with 95% bootstrap confidence intervals (10,000 resamples) computed adaptively based on distribution skew and boundedness.

Correction for Multiple Comparisons

To control the false discovery rate, we applied the Benjamini–Hochberg FDR procedure at $p = .05$, independently within each conceptually defined family of variables:

- **Temporal metrics**: duration, occurrence, duration variability for each microstate.
- **Coverage metrics**: proportion of time spent in each microstate (time coverage, %).
- **Strength metrics**: mean global field power (GFP) and GFP variability for each microstate.

- **Explained variance metrics**: total explained variance across all microstates and individual explained variance for each microstate class.
- **Transition dynamics**: observed transition probabilities (OrgTM) and chance-corrected transitions (DeltaTM), analysed together as one family. Because transition probabilities are strongly influenced by state coverage, we report both OrgTM and DeltaTM (OrgTM – expected).

Only comparisons that survived FDR correction ($p < .05$) were interpreted as statistically significant. All statistical analyses and bootstrap routines were implemented in Python using custom code.

2.5. Visualization and Taxonomic Alignment

Microstate maps and temporal-dynamic plots were visualized as PNGs for individual and group analyses. Initially, our labeling diverged from Custo et al. (2017), who assigned the salience/interoceptive network to Microstate F and the anterior-DMN/ToM network to Microstate E. However, our topographies aligned with the revised taxonomy of Tarailis et al. (2024), who corrected this inversion. Accordingly, we retained the updated labeling: Microstate E corresponds to the salience/interoceptive–emotional network, and Microstate F to the anterior-DMN/ToM network (see Figure 1). This alignment enhances interpretability and cross-study comparability of ASD-related network differences.

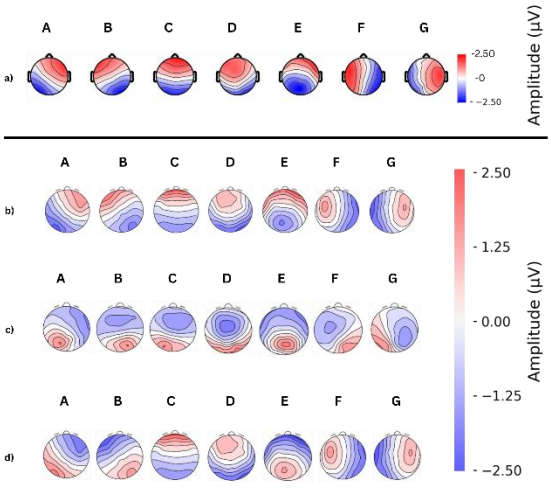

Figure 1. Comparison of canonical EEG microstate maps from Tarailis et al. (2024) and group-level maps from the present study.

(a) Grand-average microstate maps (A–G) reproduced from Taraili et al. (2024) for reference.

(b) Group-average microstates from the Low Autism Spectrum Quotient (ASQ) group.

(c) Group-average microstates from the High-ASQ group.

(d) Group-average microstates from the clinically diagnosed Autism Spectrum Disorder (ASD) group.

All scalp topographies represent voltage distributions at time points of peak Global Field Power (GFP), computed using a 7-cluster k-means solution. Maps are displayed using the same diverging colormap (RdBu) with a fixed scale of −2.5 to +2.5 μV, enabling direct visual comparison. Red indicates positive potentials; blue indicates negative potentials

3. Results

Group differences across Clinical ASD, TD-High, and TD-Low were evaluated with one-way ANOVA (when assumptions held) or Kruskal–Wallis tests otherwise. Benjamini–Hochberg false discovery rate (FDR) control ($q = .05$) was applied separately within three conceptually defined families: Temporal (mean duration, occurrence, duration variability, explained variance, GFP), Coverage (proportion of time spent in each microstate), and Transition Dynamics (observed transition probabilities, OrgTM, and chance-corrected transitions, DeltaTM). Post-hoc pairwise comparisons were conducted only for variables with a significant omnibus test ($p < .05$) and are reported here only when the corresponding pairwise contrast also survived FDR correction within its family (FDR-adjusted $p < .05$). All descriptive statistics are reported as bootstrap-based central estimates (medians or means, depending on the distribution of each measure) with 95% confidence intervals.

3.1 Mean duration and occurrence across microstates

Kruskal–Wallis tests revealed robust group differences in global temporal microstate metrics averaged across classes A–G (see Table 1). Compared with both typical groups, the clinical ASD group showed markedly shorter mean microstate durations and substantially higher occurrence rates. FDR-corrected post-hoc tests confirmed that MeanDurationAll was lower and MeanOccurrenceAll higher in ASD than in both TD-High and TD-Low (all $p < .001$, $|\text{Cliff's } \Delta| \approx 1.00$), whereas no significant differences emerged between TD-High and TD-Low on either global index.

Taken together, these results indicate that resting-state microstate sequences in clinical ASD are globally more fragmented and rapid—composed of shorter, more frequent episodes—while the two typical groups share a highly similar temporal regime.

Table 1. Global temporal microstate metrics (averaged across A–G) for Clinical ASD, TD-High, and TD-Low.

Measure	Clinical ASD (n = 28) Median [95% CI]	TD-High (n = 21) Median [95% CI]	TD-Low (n = 19) Mean [95% CI]	Kruskal–Wallis H(2)	Effect size (ε^2)	Significant FDR-adjusted pairwise differences
Mean Duration (Microstates A-G)	12.3 ms [10.9, 14.4]	40.7 ms [36.6, 41.6]	41.1 ms [39.3, 43.4]	H(2) = 48.86, p < .001	.72	ASD < TD-High; ASD < TD-Low; TD-High vs TD-Low: n.s.
Mean occurrence (events/s, Microstates A–G)	85.8 events/s [76.9, 95.2]	24.8 events/s [23.1, 26.5]	24.7 events/s [23.1, 26.4]	H(2) = 48.86, p < .001	.72	ASD > TD-High; ASD > TD-Low; TD-High vs TD-Low: n.s.

Note. Values are bootstrap-based medians with 95% confidence intervals in brackets.

Omnibus tests used Kruskal–Wallis across the three groups.

p = Benjamini–Hochberg false discovery rate–adjusted p-values for post-hoc tests within the Temporal family; only FDR-significant pairwise differences are listed.

3.2 State-specific temporal metrics

Within the Temporal family (48 variables, including mean duration, duration variability, occurrence, explained variance, and GFP measures), 31 variables showed a significant main effect of Group after FDR correction ($p < .05$). Below we summarise the state-specific temporal measures; full descriptive statistics for mean duration and occurrence are reported in Table 2, and duration variability in Table 3.

3.2.1 State-specific mean duration (Microstates A–G)

For state-specific mean duration, all seven microstates (A–G) showed robust group effects (all omnibus tests $p < .001$, all FDR-adjusted $p < .001$). Kruskal–Wallis tests were significant for Microstates A–E, and one-way ANOVAs were significant for Microstates F and G, with effect sizes (η^2/ε^2) in the moderate-to-large range (Table 2).

Across all microstates, a highly consistent pattern emerged: Clinical ASD exhibited markedly shorter mean durations than both typical groups, whereas TD-High and TD-Low did not differ significantly after FDR correction. For each microstate A–G, median durations were shortest in the Clinical ASD group and substantially longer—but comparable—across TD-High and TD-Low (all ASD vs TD-High and ASD vs TD-Low post hoc tests FDR-adjusted $p < .001$; all TD-High vs TD-Low contrasts FDR-adjusted $p \geq .05$). Median state-specific durations in Clinical ASD generally fell in the range of ~9–14 ms, compared with ~29–50 ms in both TD groups (see Table 2). For example, for Microstate E, the median mean duration was approximately 12.3 ms in Clinical ASD (95% CI [9.75, 14.36]), compared with 34.3 ms in TD-High (95% CI [32.76, 37.24]) and 30.5 ms in TD-Low (95% CI [27.93, 33.19]).

Overall, these state-specific duration findings closely mirror the global mean duration index: microstates are substantially more transient in Clinical ASD, whereas TD-High and TD-Low show similarly sustained episodes across all microstate classes (see Table 2).

Table 2. Metrics for duration and occurrence for state-specific temporal measures

Microstate	**Clinical ASD (n=28)**	**TD-High (n=21)**	**TD-Low (n=19)**	**Kruskal–Wallis H(2)**	**Effect size (ε^2)**	**Significant FDR-adjusted pairwise differences**
A	13.3 [11.6, 14.4]	38.2 [37.0, 40.6]	40.9 [36.7, 45.0]	H(2) = 49.38, p < .001	ε^2 = 0.73	ASD vs TD-High: ASD < TD-High; ASD vs TD-Low: ASD < TD-Low; TD-High vs TD-Low: n.s.

B	13.5 [11.5, 14.7]	37.8 [35.9, 44.9]	40.2 [39.4, 44.9]	H(2) = 49.10, p < .001	ε^2 = 0.72	ASD vs TD-High: ASD < TD-High; ASD vs TD-Low: ASD < TD-Low; TD-High vs TD-Low: n.s.
C	14.0 [11.9, 15.7]	49.2 [40.9, 52.2]	50.6 [46.7, 55.6]	H(2) = 48.97, p < .001	ε^2 = 0.72	ASD vs TD-High: ASD < TD-High; ASD vs TD-Low: ASD < TD-Low; TD-High vs TD-Low: n.s.
D	11.2 [8.5, 12.4]	37.0 [34.2, 40.7]	31.8 [29.5, 35.6]	H(2) = 49.57, p < .001	ε^2 = 0.73	ASD vs TD-High: ASD < TD-High; ASD vs TD-Low: ASD < TD-Low; TD-High vs TD-Low: n.s.
E	12.3 [9.8, 14.4]	34.3 [32.8, 37.2]	30.5 [27.9, 33.2]	H(2) = 49.39, p < .001	ε^2 = 0.73	ASD vs TD-High: ASD < TD-High; ASD vs TD-Low: ASD < TD-Low; TD-High vs TD-Low: n.s.

F	10.0 [9.2, 11.0]	30.8 [30.1, 33.5]	32.5 [30.2, 34.8]	F(2, 65) = 225.01, p < .001	η^2 = 0.87	ASD vs TD-High: ASD < TD-High; ASD vs TD-Low: ASD < TD-Low; TD-High vs TD-Low: n.s.
G	9.5 [7.9, 10.6]	30.7 [27.9, 32.4]	28.9 [26.5, 31.1]	F(2, 65) = 257.19, p < .001	η^2 = 0.89	ASD vs TD-High: ASD < TD-High; ASD vs TD-Low: ASD < TD-Low; TD-High vs TD-Low: n.s.

Note. Values are bootstrap-based medians or means depending on distribution, with 95% confidence intervals in brackets.

Omnibus tests used one-way ANOVA or Kruskal–Wallis, as appropriate, across the three groups.

p = Benjamini–Hochberg false discovery rate–adjusted p-values for post-hoc tests within the Temporal family; only FDR-significant pairwise differences are listed.

3.2.2 Duration variability across microstates

Duration variability (standard deviation of episode duration within each microstate class) also showed robust group effects for all microstates A–G (all $q_{(FDR,omni)} < .001$; Table 3). In general, ASD showed lower duration variability than both TD groups, consistent with a more stereotyped temporal structure.

For Microstates A, B, C, D, F, and G, ASD had significantly lower duration SD than both TD-High and TD-Low (all ASD vs TD-High and ASD vs TD-Low $p_{(FDR)} \leq .015$), while TD-High and TD-Low did not differ significantly (all $p_{(FDR)} \geq .07$). For Microstate E, all three pairwise contrasts were significant: ASD < TD-High < TD-Low (all $p_{(FDR)} \leq .014$), indicating a graded increase in duration variability along the autistic-trait continuum.

Table 3. Metrics for duration variability across microstates

Microstate	Clinical ASD (n = 28) Mean [95% CI]	TD-High (n = 21) Mean [95% CI]	TD-Low (n = 19) Mean [95% CI]	Kruskal–Wallis H(2)	Effect size (ε^2)	Significant FDR-adjusted pairwise differences
A	9.8 ms [8.2, 10.4]	23.2 ms [19.4, 25.9]	27.3 ms [22.6, 31.2]	$H(2) = 48.50$, $p < .001$	.72	ASD < TD-High; ASD < TD-Low; TD-High vs TD-Low: n.s.
B	9.8 ms [8.8, 10.9]	24.2 ms [20.4, 29.8]	29.0 ms [23.5, 33.8]	$H(2) = 44.53$, $p < .001$	.65	ASD < TD-High; ASD < TD-Low; TD-High vs TD-Low: n.s.
C	11.2 ms [10.3, 14.1]	37.6 ms [29.0, 44.0]	42.2 ms [38.6, 46.1]	$H(2) = 47.33$, $p < .001$	.70	ASD < TD-High; ASD < TD-Low; TD-High vs TD-Low: n.s.

D	7.6 ms [6.4, 9.1]	24.3 ms [20.8, 27.9]	18.6 ms [16.6, 25.2]	$H(2) = 41.77$, $p < .001$	.61	ASD < TD-High; ASD < TD-Low; TD-High vs TD-Low: n.s.
E	10.8 ms [9.8, 13.1]	20.9 ms [18.5, 23.7]	15.2 ms [12.9, 17.8]	$H(2) = 28.60$, $p < .001$	.41	ASD < TD-High; ASD < TD-Low; TD-High < TD-Low
F	8.2 ms [7.3, 9.5]	19.9 ms [16.5, 21.7]	18.9 ms [17.2, 21.9]	$H(2) = 45.31$, $p < .001$	.67	ASD < TD-High; ASD < TD-Low; TD-High vs TD-Low: n.s.
G	7.4 ms [6.2, 8.5]	18.6 ms [14.2, 20.9]	14.3 ms [13.0, 17.3]	$H(2) = 43.76$, $p < .001$	.64	ASD < TD-High; ASD < TD-Low; TD-High vs TD-Low: n.s.

Note. Values are bootstrap-based medians with 95% confidence intervals in brackets.

Omnibus tests used Kruskal–Wallis across the three groups.

p = Benjamini–Hochberg false discovery rate–adjusted p-values for post-hoc tests within the Temporal family; only FDR-significant pairwise differences are listed.

3.2.3 State-specific occurrence (Microstates A–G)

State-specific occurrence rates (events/s) for microstates A–G also showed strong group effects (all $p_{(FDR,omni)} < .001$; Table 4). The pattern inverted relative to duration: ASD showed higher

occurrence rates than both TD groups for every microstate, while TD-High and TD-Low again did not differ significantly after FDR correction.

Across microstates, ASD occurrence frequencies ranged from ~7.8–14.2 events/s, compared with ~2.0–6.1 events/s in the TD groups (Table 4). FDR-corrected post-hoc tests indicated that for each microstate A–G, ASD > TD-High and ASD > TD-Low (all $p \leq .002$), whereas TD-High vs TD-Low was non-significant for all states (all $p \geq .24$). Taken together with the duration results, this confirms a globally more fragmented and rapid microstate regime in Clinical ASD.

Table 4. Metrics for State-specific occurrence (Microstates A–G)

Microstate	Clinical ASD (n=28) Mean [95% CI]	TD-High (n=21) Mean [95% CI]	TD-Low (n=19) Mean [95% CI]	Kruskal–Wallis H(2)	Effect size (ε^2)	Significant FDR-adjusted pairwise differences
A	13.81 [12.03, 15.77]	3.81 [3.23, 4.38]	4.39 [3.85, 4.97]	H(2) = 49.00, p < .001	ε^2 = 0.72	ASD vs TD-High: ASD > TD-High; ASD vs TD-Low: ASD > TD-Low; TD-High vs TD-Low: n.s.
B	12.77 [11.52, 15.12]	3.82 [3.25, 4.36]	4.46 [4.08, 4.85]	H(2) = 49.43, p < .001	ε^2 = 0.73	ASD vs TD-High: ASD > TD-High; ASD vs TD-Low: ASD > TD-Low; TD-High vs TD-Low: n.s.

C	13.95 [12.41, 16.22]	5.04 [4.88, 5.69]	5.83 [5.34, 6.29]	H(2) = 50.24, p < .001	ε^2 = 0.74	ASD vs TD-High: ASD > TD-High; ASD vs TD-Low: ASD > TD-Low; TD-High vs TD-Low: n.s.
D	9.36 [8.17, 10.60]	3.56 [2.78, 4.37]	2.40 [1.43, 3.49]	F(2, 65) = 57.67, p < .001	η^2 = 0.64	ASD vs TD-High: ASD > TD-High; ASD vs TD-Low: ASD > TD-Low; TD-High vs TD-Low: n.s.
E	11.47 [10.40, 12.59]	3.07 [1.79, 4.24]	2.15 [1.73, 2.58]	H(2) = 47.98, p < .001	ε^2 = 0.71	ASD vs TD-High: ASD > TD-High; ASD vs TD-Low: ASD > TD-Low; TD-High vs TD-Low: n.s.
F	11.08 [8.53, 13.53]	2.80 [2.26, 3.32]	3.11 [2.69, 3.51]	H(2) = 48.92, p < .001	ε^2 = 0.72	ASD vs TD-High: ASD > TD-High; ASD vs TD-Low: ASD > TD-Low; TD-High vs TD-Low: n.s.

G	8.15 [7.63, 9.83]	2.31 [1.67, 2.60]	1.92 [1.60, 2.24]	H(2) = 46.23, p < .001	ε² = 0.68	ASD vs TD-High: ASD > TD-High; ASD vs TD-Low: ASD > TD-Low; TD-High vs TD-Low: n.s.

Note. Values are bootstrap-based medians or means depending on distribution, with 95% confidence intervals in brackets.

Omnibus tests used one-way ANOVA or Kruskal–Wallis, as appropriate, across the three groups.

p = Benjamini–Hochberg false discovery rate–adjusted p-values for post-hoc tests within the Temporal family; only FDR-significant pairwise differences are listed.

3.3 Explained variance and GFP-based strength

3.3.1 Total explained variance

Total explained variance across the seven microstates showed a robust main effect of group (Kruskal–Wallis H(2) = 24.04, $p < .001$, $\varepsilon^2 = .34$, $p_{(FDR)} = <.001$; Table 5).

Median total explained variance was lowest in the ASD group (Mdn = 0.49, 95% CI [0.46, 0.54]), and higher in both TD groups (TD-High: Mdn = 0.63, 95% CI [0.59, 0.65]; TD-Low: Mdn = 0.59, 95% CI [0.57, 0.65]).

FDR-corrected post-hoc tests confirmed that ASD had lower total explained variance than both TD-High and TD-Low, whereas TD-High and TD-Low did not differ reliably from each other (Table 5).

T*able 5. Metrics for total explained variance and individual microstate explained variance*

Microstate	Clinical ASD (n=28) Mean [95% CI]	TD-High (n=21) Mean [95% CI]	TD-Low (n=19) Mean [95% CI]	Kruskal–Wallis H(2)	Effect size (ε^2)	Significant FDR-adjusted pairwise differences
Total explained variance (A–G)	0.49 [0.46, 0.54]	0.63 [0.59, 0.65]	0.59 [0.57, 0.65]	H(2) = 24.04, p < .001	ε^2 = 0.34	ASD vs TD-High: ASD < TD-High; ASD vs TD-Low: ASD < TD-Low; TD-High vs TD-Low: n.s.
A	0.06 [0.05, 0.09]	0.08 [0.07, 0.09]	0.10 [0.08, 0.13]	F(2, 65) = 4.01, p = 0.023	η^2 = 0.11	ASD vs TD-High: n.s.; ASD vs TD-Low: ASD < TD-Low; TD-High vs TD-Low: n.s.
C	0.13 [0.11, 0.17]	0.19 [0.17, 0.24]	0.24 [0.21, 0.29]	F(2, 65) = 10.88, p < .001	η^2 = 0.25	ASD vs TD-High: ASD < TD-High; ASD vs TD-Low: ASD < TD-Low; TD-High vs TD-Low: n.s.

E	0.07 [0.05, 0.09]	0.05 [0.03, 0.09]	0.02 [0.01, 0.03]	H(2) = 17.91, p < .001	ε^2 = 0.24	ASD vs TD-High: n.s.; ASD vs TD-Low: ASD > TD-Low; TD-High vs TD-Low: TD-High > TD-Low
G	0.03 [0.02, 0.03]	0.03 [0.02, 0.03]	0.02 [0.01, 0.02]	H(2) = 7.17, p = 0.028	ε^2 = 0.08	ASD vs TD-High: n.s.; ASD vs TD-Low: ASD > TD-Low; TD-High vs TD-Low: TD-High > TD-Low

Note. Values are bootstrap-based medians or means depending on distribution, with 95% confidence intervals in brackets.

Omnibus tests used one-way ANOVA or Kruskal–Wallis, as appropriate, across the three groups.

p = Benjamini–Hochberg false discovery rate–adjusted p-values for post-hoc tests within the Explained variance family; only FDR-significant pairwise differences are listed.

3.3.2 Microstate-specific explained variance (A, C, E, G)

Explained variance for individual microstates showed significant group effects for Microstates A, C, E, and G after FDR correction within the explained-variance family (all FDR-adjusted $p \leq .041$; Table 5). Explained variance for Microstates B, D, and F did not differ significantly between groups (all FDR-adjusted $p \geq .10$) and are not discussed further.

For Microstate A (audio–visual/arousal), a one-way ANOVA revealed a small but reliable group effect in explained variance ($F(2, 65) = 4.01$, $p = .023$, $\eta^2 = .11$, FDR-adjusted $p = .035$). Median explained variance was lowest in the Clinical ASD group (Mdn = 0.06, 95% CI [0.05, 0.09]) and highest in TD-Low (Mdn = 0.10, 95% CI [0.08, 0.13]). FDR-corrected post-hoc tests confirmed a significant reduction in Microstate-A explained variance in ASD relative to TD-Low, whereas contrasts involving TD-High did not reach FDR-corrected significance (Table 5).

For Microstate C (personally significant/self-referential mentation), explained variance showed a moderate group effect ($F(2, 65) = 10.88$, $p < .001$, $\eta^2 = .25$, FDR-adjusted $p < .001$). Median

explained variance for C was lowest in ASD (Mdn = 0.13, 95% CI [0.11, 0.17]), intermediate in TD-High (Mdn = 0.19, 95% CI [0.17, 0.24]), and highest in TD-Low (Mdn = 0.24, 95% CI [0.21, 0.29]). FDR-corrected post-hoc comparisons indicated that ASD showed significantly reduced Microstate-C explained variance relative to both TD-High and TD-Low, while the two typical groups did not differ significantly (Table 5).

For Microstate E (salience/interoceptive–emotional network), a Kruskal–Wallis test indicated a pronounced group effect in explained variance ($H(2) = 17.91$, $p < .001$, $\varepsilon^2 = .24$, FDR-adjusted $p < .001$). Median values showed a graded pattern consistent with a dimensional autism–BAP continuum: TD-Low (Mdn = 0.02, 95% CI [0.01, 0.03]) < TD-High (Mdn = 0.05, 95% CI [0.03, 0.09]) < ASD (Mdn = 0.07, 95% CI [0.05, 0.09]). After FDR correction, TD-Low had significantly lower Microstate-E explained variance than both TD-High and ASD, whereas the ASD vs TD-High contrast did not differ reliably (Table 5).

For Microstate G (somatosensory/sensorimotor), explained variance also differed by group ($H(2) = 7.17$, $p = .028$, $\varepsilon^2 = .08$, FDR-adjusted $p = .041$). Explained variance was lowest in TD-Low (Mdn = 0.02, 95% CI [0.01, 0.02]) and higher in both ASD (Mdn = 0.03, 95% CI [0.02, 0.03]) and TD-High (Mdn = 0.03, 95% CI [0.02, 0.03]). FDR-corrected post-hoc tests showed that TD-Low had lower Microstate-G explained variance than both ASD and TD-High, with no reliable difference between ASD and TD-High (Table 5).

Taken together, the explained-variance results indicate a reduced contribution of Microstate C in Clinical ASD, alongside increased contributions of Microstates E and G with higher autistic traits, with TD-High typically occupying an intermediate position along the ASD–BAP spectrum.

3.3.3 GFP-based strength measures (Microstate E)

We next examined whether group differences in Microstate E extended to signal strength (mean global field power, GFP) and its variability. Within the GFP family, only Microstate E showed reliable group effects after FDR correction; mean GFP and GFP variability for Microstates A–D, F, and G did not differ significantly between groups (all FDR-adjusted $p \geq .14$).

For mean GFP in Microstate E, there was a significant main effect of group (Kruskal–Wallis $H(2) = 9.48$, $p = .009$, $\varepsilon^2 = .12$, FDR-adjusted $p = .014$). Median estimates indicated higher GFP amplitude in the Clinical ASD group (Mdn = 7.49 μV, 95% CI [6.64, 8.30]) than in both TD-High (Mdn = 5.78 μV, 95% CI [4.66, 8.11]) and TD-Low (Mdn = 5.74 μV, 95% CI [5.18, 6.27]). FDR-corrected post-hoc tests confirmed that ASD had greater mean GFP than each typical group, whereas TD-High and TD-Low did not differ significantly (see Table 6).

Table 6. Metrics for GFP-based strength measures

Measure	Clinical ASD (n=28) Mean [95% CI]	TD-High (n=21) Mean [95% CI]	TD-Low (n=19) Mean [95% CI]	Kruskal–Wallis H(2)	Effect size (ε^2)	Significant FDR-adjusted pairwise differences
Mean GFP (μV), Microstate E	7.49 [6.64, 8.30]	5.78 [4.66, 8.11]	5.74 [5.18, 6.27]	H(2) = 9.48, p = 0.009	ε^2 = 0.12	ASD vs TD-High: ASD > TD-High; ASD vs TD-Low: ASD > TD-Low; TD-High vs TD-Low: n.s.
GFP SD (μV), Microstate E	3.47 [2.79, 4.19]	2.19 [1.77, 3.12]	2.12 [1.85, 2.38]	H(2) = 10.03, p = 0.007	ε^2 = 0.12	ASD vs TD-High: ASD > TD-High; ASD vs TD-Low: ASD > TD-Low; TD-High vs TD-Low: n.s.

Note. Values are bootstrap-based medians with 95% confidence intervals in brackets.

Omnibus tests used Kruskal–Wallis across the three groups.

p = Benjamini–Hochberg false discovery rate–adjusted p-values for post-hoc tests within the Strength metrics family; only FDR-significant pairwise differences are listed.

GFP variability in Microstate E showed a similar pattern. GFPStdDev_E differed across groups (H(2) = 10.03, p = .007, ε^2 = .12, FDR-adjusted p = .011), with the Clinical ASD group again showing the highest variability (Mdn = 3.47 μV, 95% CI [2.79, 4.19]) relative to TD-High (Mdn = 2.19 μV, 95% CI [1.77, 3.12]) and TD-Low (Mdn = 2.12 μV, 95% CI [1.85, 2.38]). FDR-adjusted post-hocs indicated greater GFP variability in ASD than in both TD groups, with no reliable difference between TD-High and TD-Low (Table 6).

Taken together with the explained-variance and coverage results, these findings reinforce Microstate E as a central locus of group differences: in Clinical ASD, this salience/interoceptive state not only accounts for a larger proportion of variance, but is also expressed with stronger and more variable GFP than in either typical group, while TD-High again occupies an intermediate, BAP-consistent position.

3.4 Spatial coverage

Within the Coverage family (proportion of time spent in each microstate), FDR-corrected omnibus tests ($p < .05$ within family) indicated reliable group effects **only** for Microstates C, E, and G (Table 7). Coverage for Microstates A, B, D, and F did not differ significantly between groups after FDR correction (all $p > .05$).

For Microstate C, a Kruskal–Wallis test showed a robust group effect, $H(2) = 22.58$, $p < .001$, $\varepsilon^2 \approx .32$. Central estimates indicated that Clinical ASD spent the least time in C (ASD: ≈19.2% of recording, 95% CI [17.7, 20.9]), compared with both TD groups (TD-High: ≈26.5%, 95% CI [23.2, 29.6]; TD-Low: ≈29.7%, 95% CI [27.3, 31.0]). FDR-corrected Dunn tests ($p < .05$) showed that ASD spent significantly less time in C than both TD-High and TD-Low, whereas TD-High and TD-Low did not differ reliably.

For Microstate E, there was again a significant group effect, $H(2) = 17.26$, $p < .001$, $\varepsilon^2 \approx .23$. Coverage showed a graded pattern along the autism–BAP continuum: ASD spent the most time in E (≈12.4%, 95% CI [10.4, 14.9]), followed by TD-High (≈10.3%, 95% CI [7.2, 13.8]) and TD-Low (≈6.0%, 95% CI [4.6, 7.7]). Post-hoc tests revealed that TD-Low spent significantly less time in Microstate E than both ASD and TD-High ($p < .05$), whereas the difference between ASD and TD-High did not survive FDR correction.

For Microstate G, group differences were again reliable, $H(2) = 16.15$, $p < .001$, $\varepsilon^2 \approx .22$. Coverage was highest in ASD (≈9.1%, 95% CI [8.1, 10.3]), intermediate in TD-High (≈7.2%, 95% CI [5.8, 8.5]), and lowest in TD-Low (≈5.7%, 95% CI [5.0, 6.2]). FDR-adjusted post-hoc comparisons indicated that ASD showed greater coverage of G than both TD groups (ASD > TD-High and ASD > TD-Low, both $p < .05$), whereas TD-High and TD-Low did not differ significantly after correction.

Taken together, coverage results converge with the explained-variance findings: Clinical ASD is characterised by reduced time in Microstate C and increased occupancy of Microstates E and G, with TD-High generally showing an intermediate but more “BAP-like” pattern than TD-Low. Statistics for coverage measures are reported below in Table 7.

Table 7. Metrics for Spatial coverage

Microstate	Clinical ASD (n = 28) Mean [95% CI]	TD-High (n = 21) Mean [95% CI]	TD-Low (n = 19) Mean [95% CI]	Kruskal–Wallis H(2)(Kruskal–Wallis)	Effect size ε^2	Significant FDR-adjusted pairwise differences within Coverage family
A	16.8% [15.3, 17.5]	14.9% [12.6, 17.2]	18.1% [15.7, 20.4]	H(2) = 4.57, p = .102, p = .129	.04	None (omnibus n.s. after FDR)
B	18.0% [16.7, 19.3]	15.7% [12.8, 18.6]	18.8% [16.7, 20.8]	H(2) = 2.75, p = .253, p = .253	.01	None (omnibus n.s. after FDR)
C	19.2% [17.7, 20.9]	26.5% [21.8, 31.5]	29.7% [26.6, 32.6]	H(2) = 22.58, p < .001, p = .00009	.32	ASD < TD-High; ASD < TD-Low; TD-High vs TD-Low: n.s.
D	9.9% [8.9, 11.8]	13.7% [10.4, 17.2]	8.2% [5.3, 11.9]	H(2) = 4.40, p = .111, p = .129	.04	None (omnibus n.s. after FDR)

E	12.4% [11.3, 15.9]	10.3% [6.1, 14.4]	6.0% [4.6, 8.2]	H(2) = 17.26, p < .001, p = .00062	.23	TD-Low < ASD; TD-Low < TD-High; ASD vs TD-High: n.s.
F	11.8% [10.9, 12.8]	9.1% [7.4, 10.9]	10.2% [8.9, 11.4]	H(2) = 6.33, p = .042, p = .074	.07	None (p ≥ .05; treated as n.s. after FDR)
G	9.1% [8.2, 10.1]	7.2% [5.1, 8.4]	5.7% [4.8, 6.6]	H(2) = 16.15, p < .001, p = .00073	.22	ASD > TD-High; ASD > TD-Low; TD-High vs TD-Low: n.s.

Note. Values are bootstrap-based medians with 95% confidence intervals in brackets.

Omnibus tests used Kruskal–Wallis across the three groups.

p = Benjamini–Hochberg false discovery rate–adjusted p-values for post-hoc tests within the Coverage family; only FDR-significant pairwise differences are listed.

3.5 Transition dynamics

The TransitionDynamics family comprised 84 variables: 42 observed transition probabilities (OrgTM; e.g., OrgTM_A→B) and 42 chance-corrected transitions (ΔTM; e.g., DeltaTM_A→B).

After Benjamini–Hochberg FDR correction of omnibus tests within this family, 32 OrgTM and 21 ΔTM edges showed reliable group effects ($p < .05$). Within these omnibus-significant transitions, FDR-adjusted post-hoc tests indicated that Clinical ASD differed from TD-Low on the majority of edges, with fewer but still systematic differences between TD-High and TD-Low, and only a subset of transitions distinguishing Clinical ASD from TD-High. This pattern is consistent with an intermediate, broader-autism-phenotype profile in TD-High.

3.5.1 Observed transition probabilities (OrgTM)

A first set of robust effects involved the short-range "ping-pong" among early sensory/attentional microstates A, B, and C. All six directed transitions within this ensemble (A→B, A→C, B→A, B→C, C→A, C→B) showed significant omnibus group differences (all $p < .05$; Table 8). FDR-corrected post-hoc tests consistently indicated that TD-Low had higher transition probabilities than both Clinical ASD and TD-High for every A–C edge, whereas Clinical ASD and TD-High did not differ significantly from each other on any of these transitions. Bootstrapped group estimates showed that TD-Low always had the highest transition probabilities, with ASD and TD-High showing similarly reduced short-range recurrences (ASD lowest or comparable to TD-High; Table 8). Thus, short-range sensory recurrences within the A–C ensemble are most prominent in TD-Low and attenuated in both Clinical ASD and TD-High.

A second cluster of OrgTM effects involved loops linking higher-order microstates D and E with the sensorimotor map G (Table 8). For the D↔E loop (D→E, E→D), omnibus tests were significant and FDR-corrected post-hoc comparisons showed that TD-Low had lower transition probabilities than both Clinical ASD and TD-High, whereas ASD and TD-High did not differ significantly from each other. Bootstrapped estimates followed a graded pattern TD-Low < ASD < TD-High for both directions, suggesting that higher-order cycling between D and E is particularly enhanced in TD-High, with ASD intermediate and TD-Low lowest. For transitions between E and G (E→G, G→E), median transition probabilities increased along a TD-Low < TD-High < ASD continuum. FDR-corrected post-hoc tests indicated that ASD had higher E–G coupling than both TD groups, whereas TD-Low and TD-High did not differ reliably, again pointing to especially strong E–G coupling in Clinical ASD. For G→D, TD-Low also showed the lowest transition probability, and ASD exhibited significantly stronger G→D routing than TD-Low, while TD-High was descriptively higher than TD-Low but did not differ significantly from either group after FDR correction.

Taken together, the OrgTM findings show that Clinical ASD is characterised by attenuated short-range sensory "ping-pong" within the A–C ensemble and enhanced routing between higher-order (D/E) and sensorimotor (G) states. TD-High differs reliably from TD-Low on all A–C transitions and on the D↔E loop, and often occupies an intermediate or more "ASD-like" position for D/E/G edges, consistent with broader-autism-phenotype variation in network routing.

Table 8. Summary of metrics for OrgTM edges

Transition	Clinical ASD (n = 28)	TD-High (n = 21)	TD-Low (n = 19)	Omnibus test	ε^2	Significant FDR-adjusted pairwise differences (q_adj < .05)
A→B	1.99 [1.77, 2.28]	2.41 [1.90, 3.38]	3.72 [3.03, 4.43]	H(2) = 14.05, p < .001	0.19	TD-Low > ASD; TD-Low > TD-High
A→C	3.83 [3.34, 4.68]	4.13 [3.11, 5.32]	6.20 [5.22, 7.14]	H(2) = 10.06, p = .007	0.12	TD-Low > ASD; TD-Low > TD-High
B→A	2.02 [1.78, 2.41]	2.19 [1.81, 3.32]	3.66 [3.00, 4.32]	H(2) = 12.32, p = .002	0.16	TD-Low > ASD; TD-Low > TD-High
B→C	4.34 [4.00, 4.69]	4.19 [3.66, 5.39]	6.70 [5.57, 7.84]	H(2) = 11.54, p = .003	0.15	TD-Low > ASD; TD-Low > TD-High
C→A	3.90 [3.12, 4.63]	4.07 [3.23, 5.21]	6.14 [5.13, 7.11]	H(2) = 11.07, p = .004	0.14	TD-Low > ASD; TD-Low > TD-High
C→B	4.35 [3.98, 4.71]	4.04 [3.71, 5.58]	6.54 [5.42, 7.60]	H(2) = 9.92, p = .007	0.12	TD-Low > ASD; TD-Low > TD-High
D→E	1.70 [1.53, 1.91]	2.42 [1.03, 3.17]	0.91 [0.57, 1.62]	H(2) = 9.02, p = .011	0.11	TD-Low < ASD; TD-Low < TD-High

E→D	1.72 [1.55, 1.89]	1.93 [1.04, 3.07]	0.77 [0.42, 1.55]	H(2) = 8.58, p = .014	0.10 TD-Low < ASD; TD-Low < TD-High
E→G	1.97 [1.73, 2.20]	1.11 [0.87, 1.86]	0.80 [0.59, 1.01]	H(2) = 24.02, p < .001	0.34 ASD > TD-High; TD-Low < ASD
G→E	2.06 [1.83, 2.29]	1.21 [0.79, 1.63]	0.76 [0.54, 0.99]	H(2) = 29.57, p < .001	0.42 ASD > TD-High; TD-Low < ASD
G→D	1.86 [1.62, 2.11]	2.10 [0.89, 2.28]	1.10 [0.54, 1.44]	H(2) = 8.01, p = .018	TD-Low < ASD 0.09

Note. Values are bootstrap-based medians with 95% confidence intervals in brackets.

Omnibus tests used Kruskal–Wallis across the three groups.

p = Benjamini–Hochberg false discovery rate–adjusted p-values for post-hoc tests within the Transition dynamics family; only FDR-significant pairwise differences are listed.

3.5.2 Chance-corrected transitions (ΔTM)

To account for differences in microstate coverage, we next examined chance-corrected transitions (ΔTM = OrgTM − expected), which quantify deviations from a null model based on each state's base rate. Within the TransitionDynamics family, 21 ΔTM edges showed significant omnibus effects after FDR correction. Of these, 19 distinguished ASD from TD-Low, 16 distinguished ASD from TD-High, and 4 distinguished TD-High from TD-Low at the FDR-adjusted level. Overall, the ΔTM pattern closely mirrored the OrgTM results, indicating that group differences reflect genuine reorganisation of routing structure rather than trivial consequences of time spent in each state.

The four ΔTM edges that differentiated TD-High from TD-Low after FDR correction were B→E, D→B, E→B, and G→E. All of these also showed significant differences between ASD and TD-Low, whereas ASD and TD-High did not differ significantly after FDR correction on any of these edges. Bootstrapped estimates indicated that ΔTM B→E deviations were most negative

in TD-Low, less negative in TD-High, and least negative in ASD, implying that transitions from B to E are most strongly under-expressed relative to chance in TD-Low, with both ASD and TD-High showing reduced suppression. For D→B, ΔTM was strongly negative in both ASD and TD-High but only mildly negative in TD-Low, suggesting that returns from D to B are markedly under-expressed in ASD and TD-High compared with TD-Low. For E→B, TD-Low showed clear under-expression, ASD values were close to chance, and TD-High exhibited a slight positive deviation, indicating that ASD and TD-High both deviate from TD-Low in the same direction, with TD-High showing the strongest relative preference for E→B. Finally, for G→E, deviations were negative in TD-Low, positive in TD-High, and strongly positive in ASD, indicating that routing from G to E is favoured above chance in ASD and TD-High but under-expressed in TD-Low. Across these four edges, effect sizes for TD-High–TD-Low and ASD–TD-Low contrasts were again large, supporting robust differences in chance-corrected routing relative to TD-Low.

For the remaining ΔTM edges, FDR-significant post-hoc effects primarily contrasted ASD with both typical groups, with TD-High generally showing intermediate deviations that followed the same direction as ASD. In particular, short-range sensory recurrences (A↔B, C↔A/B) were under-expressed relative to chance in ASD compared with both TD groups, while several sensory/sensorimotor → higher-order routes showed more positive ΔTM in ASD, consistent with preferential routing from sensory and sensorimotor states into salience and higher-order networks once base rates were controlled.

Overall, the ΔTM results reinforce the OrgTM findings: short-range sensory loops are specifically under-expressed in Clinical ASD, whereas routes from sensory and sensorimotor microstates into salience and other higher-order networks (e.g., B→E, G→E) are relatively favoured. TD-High again occupies an intermediate position between TD-Low and ASD, showing attenuated but directionally similar deviations, consistent with a dimensional broader-autism-phenotype account. Key ΔTM edges are summarised in Table 9.

Table 9. Summary of metrics for ΔTM edges

Edge (ΔTM)	**Kruskal–Wallis H(2)**	**Effect size (ε^2/η^2)**	**FDR-significant pairwise differences**

A→B	$H(2) = 24.20$, $p < .001$	0.34	ASD < TD-Low; ASD < TD-High; TD-High vs TD-Low: n.s.
A→C	$H(2) = 12.02$, $p = 0.002$	0.15	ASD > TD-Low; ASD > TD-High; TD-High vs TD-Low: n.s.
A→D	$H(2) = 10.71$, $p = 0.005$	0.13	ASD < TD-Low; ASD < TD-High; TD-High vs TD-Low: n.s.
A→F	$H(2) = 25.80$, $p < .001$	0.37	ASD > TD-Low; ASD > TD-High; TD-High vs TD-Low: n.s.
B→A	$F(2, 65) = 14.65$, $p < .001$	0.31	ASD < TD-Low; ASD < TD-High; TD-High vs TD-Low: n.s.
B→E	$F(2, 65) = 8.86$, $p < .001$	0.21	ASD > TD-Low; ASD vs TD-High: n.s.; TD-High > TD-Low
B→F	$H(2) = 20.06$, $p < .001$	0.28	ASD > TD-Low; ASD > TD-High; TD-High vs TD-Low: n.s.

C→A	H(2) = 30.07, p < .001	0.43	ASD > TD-Low; ASD > TD-High; TD-High vs TD-Low: n.s.
C→B	H(2) = 22.57, p < .001	0.32	ASD > TD-Low; ASD > TD-High; TD-High vs TD-Low: n.s.
C→F	H(2) = 21.05, p < .001	0.29	ASD < TD-Low; ASD < TD-High; TD-High vs TD-Low: n.s.
C→G	F(2, 65) = 21.87, p < .001	0.40	ASD < TD-Low; ASD < TD-High; TD-High vs TD-Low: n.s.
D→B	F(2, 65) = 3.85, p = 0.026	0.11	ASD < TD-Low; ASD vs TD-High: n.s.; TD-High vs TD-Low: n.s.
D→F	H(2) = 8.05, p = 0.018	0.09	ASD > TD-Low; ASD vs TD-High: n.s.; TD-High vs TD-Low: n.s.
D→G	H(2) = 13.66, p = 0.001	0.18	ASD > TD-Low; ASD > TD-High; TD-High vs TD-Low: n.s.

E→B	F(2, 65) = 4.01, p = 0.023	0.11	ASD vs TD-Low: n.s.; ASD vs TD-High: n.s.; TD-High > TD-Low
F→A	F(2, 65) = 15.66, p < .001	0.33	ASD > TD-Low; ASD > TD-High; TD-High vs TD-Low: n.s.
F→B	H(2) = 10.61, p = 0.005	0.13	ASD vs TD-Low: n.s.; ASD > TD-High; TD-High vs TD-Low: n.s.
F→C	H(2) = 26.36, p < .001	0.37	ASD < TD-Low; ASD < TD-High; TD-High vs TD-Low: n.s.
G→B	F(2, 65) = 5.54, p = 0.006	0.15	ASD vs TD-Low: n.s.; ASD > TD-High; TD-High vs TD-Low: n.s.
G→C	F(2, 65) = 42.41, p < .001	0.57	ASD < TD-Low; ASD < TD-High; TD-High vs TD-Low: n.s.
G→E	H(2) = 14.38, p < .001	0.19	ASD > TD-Low; ASD vs TD-High: n.s.; TD-High > TD-Low

Note. Values are bootstrap-based medians or means depending on distribution, with 95% confidence intervals in brackets.

Omnibus tests used one-way ANOVA or Kruskal–Wallis, as appropriate, across the three groups.

p = Benjamini–Hochberg false discovery rate–adjusted p-values for post-hoc tests within the Transition dynamics family; only FDR-significant pairwise differences are listed.

4. Discussion

This study compared resting-state EEG microstate dynamics in adults with clinical autism spectrum disorder (ASD) and typically developing adults with high (TD-High) and low (TD-Low) autistic traits. Using a seven-class microstate taxonomy and a hierarchical inferential framework (omnibus tests → gated post-hoc comparisons → Benjamini–Hochberg FDR control within variable families), we identified robust group differences in temporal, spatial, and transition-based metrics.

Overall, Clinical ASD was characterised by a globally more fragmented and stereotyped microstate regime, shorter but more frequent microstate episodes with reduced duration variability, alongside pronounced alterations in microstates linked to salience/interoception (E), self-referential DMN processing (C), and somatosensory/sensorimotor processing (G). TD-High participants showed fewer and more selective departures from TD-Low, typically in metrics linked to Microstates E and G and in specific transition edges, consistent with an intermediate position on the broader autism phenotype (BAP) rather than a simple "subclinical copy" of clinical ASD.

4.1 Temporal and spatial microstate dynamics

The most striking temporal finding was a global shift in Clinical ASD toward shorter and more frequent microstate episodes. Across all seven classes, clinical participants showed markedly reduced mean microstate duration, increased occurrence rates, and lower duration variability relative to both TD groups, with effect sizes (Cliff's Δ) close to ±1.00 and no differences between TD-High and TD-Low. Together, these global indices suggest that large-scale brain states in ASD enter and exit more rapidly and with less temporal diversity, consistent with a more fragmented and stereotyped temporal organisation of resting-state network dynamics.

At the state-specific level, FDR-corrected omnibus tests revealed group effects in mean duration and occurrence for all microstates (A–G), with a highly consistent pattern in the post-hoc contrasts: for each class, Clinical ASD showed shorter duration and higher occurrence than both TD-High and TD-Low, whereas no duration or occurrence differences between the two TD groups was exhibited. This indicates that the global fragmentation of microstates in ASD is not driven by a single aberrant state but reflects a system-wide temporal reconfiguration of canonical microstate classes—including A (multimodal auditory–visual/arousal-related), B (self-related visual/autobiographical), C (self-referential DMN), D (executive), E (salience/interoceptive), F (DMN/mental simulation/ToM), and G (somatosensory/sensorimotor) as synthesised in recent meta-analytic taxonomy (Tarailis et al., 2024).

Explained-variance metrics provided a more network-selective picture. Total explained variance across all microstates was significantly lower in Clinical ASD than in both TD groups, suggesting that canonical microstate templates captured a smaller proportion of scalp-EEG variance in the clinical cohort. At the level of individual classes, Microstate C showed reliably reduced explained variance in Clinical ASD relative to both TD groups, whereas Microstates E and G showed the opposite pattern: explained variance was lowest in TD-Low, higher in TD-High, and highest (or comparably high) in Clinical ASD. These graded differences in E and G (especially the TD-Low < TD-High < ASD pattern for Microstate E) are consistent with a BAP-like continuum in which salience/interoceptive and somatosensory/sensorimotor dominance increases with autistic traits.

Spatial coverage metrics converged on a similar story. After FDR correction within the Coverage family, Microstate C coverage was reduced in Clinical ASD relative to both TD-High and TD-Low, while Microstates E and G showed increased coverage in Clinical ASD and, to a lesser extent, in TD-High compared with TD-Low. Again, TD-High typically occupied an intermediate position, but many TD-High vs TD-Low contrasts did not reach FDR-corrected significance, indicating that subclinical differences are subtler and more patchy than the robust clinical–typical contrasts.

Finally, GFP-based strength metrics for Microstate E (mean GFP and GFP variability) showed selective amplification in Clinical ASD relative to both TD groups, whereas the two TD groups did not differ significantly after FDR correction. This combination—greater explained variance, increased spatial coverage, stronger amplitude, and higher GFP variability—indicates that the salience/interoceptive microstate is both more dominant and more labile in Clinical ASD, even at rest. By contrast, Microstate F, associated with DMN-related mental simulation and Theory of Mind, showed no robust differences in explained variance or spatial coverage and only a modest subset of altered transitions, despite sharing the global temporal fragmentation pattern observed across all microstates. This suggests that ToM-related network alterations may be more prominent in task-based contexts than in spontaneous eyes-closed resting activity.

4.2 Transition dynamics and large-scale routing of sensory information

Transition analyses, corrected for multiplicity within the TransitionDynamics family, revealed widespread group differences in both observed transition probabilities (OrgTM) and chance-corrected transitions (DeltaTM).

For OrgTM, the largest and most consistent differences involved transitions originating from microstates A, B, and C, which, under the updated taxonomy, jointly index early multimodal sensory/arousal (A), self-related visual/autobiographical imagery (B), and self-referential DMN processing (C). Relative to TD-Low, Clinical ASD showed reduced bidirectional transitions within this A–B–C ensemble (e.g., A↔B, A↔C, B↔C) and increased transitions from A and B into higher-order networks, including those expressed by microstates C, E, F, and G. Similar—but not identical—patterns emerged when comparing Clinical ASD with TD-High, with ASD

showing systematically higher A→F/G, B→E/F/G, and C→F/G transition probabilities and altered routing via Microstate G.

The DeltaTM results recapitulated these findings in terms of deviations from chance structure. In Clinical ASD, A↔B and C↔A/B transitions showed more negative deviations than in both TD groups (occurring less often than expected given marginal frequencies), whereas A→C/F, B→E/F/G, and C→F/G transitions showed more positive deviations, signifying preferential, above-chance routing from A/B/C into salience/interoceptive (E), DMN/ToM-related (F), and somatosensory/sensorimotor (G) microstates. TD-High again showed fewer and more selective deviations from TD-Low, mostly restricted to a subset of edges linking perceptual/self-related and higher-order states (e.g., B↔E, G→E), consistent with a weaker but directionally similar pattern to Clinical ASD.

Taken together, FDR-corrected OrgTM and DeltaTM analyses indicate that Clinical ASD is not only characterised by altered amounts of time in specific microstates but also by a qualitatively different routing architecture. Short-range transitions within the A–B–C ensemble are downweighted, whereas longer-range transitions from these perceptual/self-related states into salience, DMN, and somatosensory/sensorimotor states are upweighted. Notably, short-range A–B–C loops are most prominent in TD-Low, attenuated in TD-High, and most strongly reduced in Clinical ASD, whereas chance-corrected transitions from B and G into E show the opposite graded pattern (TD-Low < TD-High < ASD), further supporting a BAP-like continuum in routing structure. . This dynamic routing pattern fits well with triple-network accounts of ASD.

4.3 Neurobiological and clinical implications

The pattern of results reinforces a central role for the salience/interoceptive microstate E in autism. Across multiple independent metrics, explained variance, coverage, GFP amplitude and variability, and transition structure, Microstate E shows robust, convergent alterations in Clinical ASD, with TD-High often falling between TD-Low and ASD for the more tonic measures (e.g., coverage and explained variance). This combination is compatible with hyperactive yet unstable salience processing, which may underpin heightened interoceptive sensitivity, stress reactivity, and sensory overload frequently reported in ASD.

In parallel, Microstate C, indexing self-referential DMN processing, shows reduced explained variance and coverage in Clinical ASD, consistent with previous reports of atypical DMN engagement and self-related mentation in autism. The fact that microstates A and B (multimodal sensory/arousal and self-related visual/autobiographical, respectively) increasingly route into E, C, and F may reflect non-canonical integration of sensory input with self-referential and interoceptive networks, potentially contributing to difficulties in filtering and prioritising incoming stimuli.

Microstate G, putatively linked to somatosensory/sensorimotor processing, also shows graded increases in explained variance and coverage across the autism–BAP continuum. This is

compatible with findings of atypical sensorimotor involvement in ASD, and, in the context of the current transition results, suggests that perceptual and bodily information may be over-routed into somatosensory and salience networks, potentially contributing to motor restlessness and heightened bodily awareness or discomfort.

From a clinical perspective, these findings highlight Microstate E and the sensory/self-related → salience/DMN/somatosensory transition architecture as particularly promising resting-state markers for ASD. The observed pattern in TD-High participants—who often show intermediate values for Microstates E and G but largely typical global temporal metrics—supports the view that EEG microstates capture neural endophenotypes linked to the broader autism phenotype. However, the intermediate pattern is not uniform across all measures: some indices (e.g., global duration, global occurrence) showed clear clinical–typical separation with little evidence of graded subclinical disruption. This suggests that BAP-related alterations may manifest in specific network components (e.g., salience and somatosensory) and at the level of connectivity/transition structure rather than as a uniform shift of the entire microstate regime.

4.4 Methodological strengths and limitations

Several methodological features strengthen the interpretability of these findings. First, we integrated clinical and subclinical cohorts within a unified analytical framework, using a contemporary seven-class microstate taxonomy anchored in recent meta-analytic synthesis and explicit mapping to large-scale functional networks (Tarailis et al., 2024).

At the same time, important limitations must be acknowledged. Sample sizes were modest, particularly for the TD-High and TD-Low groups, which limits statistical power for detecting subtler BAP effects and increases uncertainty around some estimates, even with bootstrap CIs. The ASD dataset was drawn from a previously published cohort, whereas the TD groups were collected locally. Although we harmonised preprocessing as far as possible (e.g., identical filtering, re-referencing, 25-channel montage, and a uniform 120 s artefact-free segment per participant), differences in recruitment context, recording hardware, or environmental conditions cannot be fully excluded as residual sources of variance. We partially mitigate this by focusing on relative group differences and by using non-parametric and robust statistics, but cross-cohort integration remains a limitation.

A key limitation of the present study concerns potential confounding effects of both age and data source. The clinical ASD group was substantially older than the TD-High and TD-Low groups and was drawn from a different dataset, whereas the two typical groups were younger and collected locally using identical procedures. Age is known to influence EEG microstate parameters, including microstate duration, coverage, and transition structure, and has been identified as a major moderator of ASD-related microstate effects in prior meta-analyses (Wei et al., 2025). In addition, subtle differences in recording context, participant characteristics, and unmeasured site-specific factors may have contributed to group differences beyond diagnostic status or autistic traits per se.

Critically, the open-access dataset used for the clinical ASD group does not provide individual-level demographic information (e.g., participant-by-participant age, sex., etc). In the primary publication describing and/or citing this dataset, demographic information is reported only in aggregate (means, ranges, and standard deviations), rather than at the level of each participant. As a result, we were unable to include these variables as covariates, conduct demographic matching, or perform stratified sensitivity analyses to statistically control for potential demographic confounding between cohorts.

Although we harmonised preprocessing, channel montage, epoch length, and microstate analysis pipelines across datasets, residual cohort effects cannot be fully ruled out. Consequently, the observed group differences, particularly the pronounced temporal fragmentation in the ASD group, should be interpreted with caution, and future studies should prioritise age-matched, single-site designs and/or open datasets that include individual-level demographics to more definitively isolate autism-related microstate alterations from developmental and dataset-specific influences.

In addition, while we stratified TD participants into high- and low-trait groups using the Autism-Spectrum Quotient (AQ), the sample size was not sufficient to support fine-grained correlational analyses between continuous AQ scores and microstate metrics. Our design was optimised for detecting group-level differences across ASD, TD-High and TD-Low, rather than for high-dimensional correlational modelling. We therefore interpret TD-High vs TD-Low differences as proof-of-concept evidence for BAP-related modulation of microstate dynamics, and see comprehensive AQ–microstate correlation analyses as an important target for future, larger-scale studies.

Finally, all data were collected in a resting-state condition. This is well suited to characterising baseline network dynamics but may underestimate differences in networks such as the DMN/ToM-related Microstate F, which is typically more engaged during social-cognitive tasks. Our findings for Microstate F should therefore be interpreted as resting-state boundaries on these processes rather than an exhaustive account of mentalising network function in ASD.

4.5 Future directions

Future work can address these limitations in several ways. Larger, prospectively collected cohorts spanning the full range of autistic traits (and including more detailed symptom and sensory profiles) would allow robust dimensional analyses of AQ–microstate relationships and the mapping of specific symptom clusters onto microstate features. Incorporating task-based paradigms probing social cognition, interoception, and sensory processing would clarify when and how Microstates E, F, and G are differentially engaged and how resting-state abnormalities translate into task-evoked network dynamics.

Methodologically, the present results provide a principled basis for feature selection in machine-learning pipelines, where microstate temporal metrics, coverage, and transition patterns might be

combined with other EEG features (e.g., spectral or connectivity metrics) to develop multivariate biomarkers for ASD and BAP traits. Longitudinal designs could further test whether salience-network microstate measures, particularly Microstate E dominance and sensory/self-related → salience/DMN transition biases, serve as stable trait markers or change with intervention, making them candidates for treatment monitoring.

4.6 Conclusion

Using a rigorous analysis of seven-class EEG microstates aligned with contemporary taxonomy, this study demonstrates that Clinical ASD is characterised by globally fragmented microstate dynamics, reduced expression of self-referential DMN microstate C, and pronounced amplification of salience (Microstate E) and somatosensory/sensorimotor (Microstate G) networks, including altered routing from multimodal and self-related microstates A and B into these systems. TD-High individuals often show intermediate values for key metrics, particularly in Microstates E and G and in selected transitions, consistent with a dimensional, BAP-consistent model rather than a categorical split between "clinical" and "typical" brains.

Our findings strengthen the evidence that salience/interoceptive dysregulation and altered sensory/self-related → higher-order transition structure are core features of autism-related large-scale brain dynamics at rest. EEG microstates therefore represent a promising, low-cost tool for probing these dynamics across the autism spectrum and for developing translational markers for early identification and intervention monitoring.

Funding Acknowledgement

This research was supported by a PhD scholarship from the Consejo Nacional de Ciencia y Tecnología (CONACYT), Mexico.

Declaration of Generative AI in scientific writing

During the preparation of this work the author(s) used ChatGPT in order to improve the readability and language of the manuscript. After using this tool/service, the author(s) reviewed and edited the content as needed and take full responsibility for the content of the published article.

1. References

American Psychiatric Association. (2013). Diagnostic and statistical manual of mental disorders (5th ed.). American Psychiatric Publishing.

Attanasio, M., Mazza, M., Donne, I. L., Nigri, A., & Valenti, M. (2024). Salience Network in

Autism: preliminary results on functional connectivity analysis in resting state. European Archives of Psychiatry and Clinical Neuroscience. https://doi.org/10.1007/s00406-024-01949-y

Ayub, R., Sun, K. L., Flores, R. E., Lam, V. T., Jo, B., Saggar, M., & Fung, L. K. (2021). Thalamocortical connectivity is associated with autism symptoms in high-functioning adults with autism and typically developing adults. Translational Psychiatry, 11(1). https://doi.org/10.1038/s41398-021-01221-0

Baran, B., Nguyen, Q. T. H., Mylonas, D., Santangelo, S. L., & Manoach, D. S. (2022). Increased resting-state thalamocortical functional connectivity in children and young adults with autism spectrum disorder. Autism Research, 16(2), 271–279. https://doi.org/10.1002/aur.2875

Baron-Cohen, S., Wheelwright, S., Skinner, R., Martin, J., & Clubley, E. (2001). The Autism-Spectrum Quotient (AQ): Evidence from Asperger syndrome/high-functioning autism, males and females, scientists and mathematicians. Journal of Autism and Developmental Disorders, 31(1), 5–17. https://doi.org/10.1023/A:1005653411471

Bréchet, L., & Michel, C. M. (2022). EEG microstates in altered states of consciousness. Frontiers in Psychology, 13, 856697. https://doi.org/10.3389/fpsyg.2022.856697

Croce, P., Quercia, A., Costa, S., & Zappasodi, F. (2020). EEG microstates associated with intra- and inter-subject alpha variability. Scientific Reports, 10, 2469. https://doi.org/10.1038/s41598-020-58787-w

Custo, A., Van De Ville, D., Wells, W. M., Tomescu, M. I., Brunet, D., & Michel, C. M. (2017). Electroencephalographic resting-state networks: Source localization of microstates. Brain Connectivity, 7(10), 671–682. https://doi.org/10.1089/brain.2017.0527

D'Croz-Baron, D. F., Baker, M., Michel, C. M., & Karp, T. (2019). EEG microstates analysis in young adults with autism spectrum disorder during resting-state. Frontiers in Human Neuroscience, 13, 173. https://doi.org/10.3389/fnhum.2019.00173

Dajani, D. R., & Uddin, L. Q. (2016). Demystifying cognitive flexibility: Implications for clinical and developmental neuroscience. Trends in Neurosciences, 38(9), 571–578. https://doi.org/10.1016/j.tins.2015.07.003

Das, S., Zomorrodi, R., Enticott, P. G., Kirkovski, M., Blumberger, D. M., Rajji, T. K., & Desarkar, P. (2022). Resting state electroencephalography microstates in autism spectrum disorder: A mini-review. Frontiers in Psychiatry, 13, 988939. https://doi.org/10.3389/fpsyt.2022.988939

Das, S., Zomorrodi, R., Kirkovski, M., Hill, A. T., Enticott, P. G., Blumberger, D. M., ... & Desarkar, P. (2024). Atypical alpha band microstates produced during eyes-closed resting state EEG in autism. Progress in Neuro-Psychopharmacology and Biological Psychiatry, 131, 110958. https://doi.org/10.1016/j.pnpbp.2024.110958

Dickinson, A., Jeste, S., & Milne, E. (2022). Electrophysiological signatures of brain aging in autism spectrum disorder. Cortex, 148, 139–151. https://doi.org/10.1016/j.cortex.2021.09.022

Feng, D., & Cliff, N. (2004). Monte Carlo evaluation of ordinal d with improved variance estimation. Journal of Modern Applied Statistical Methods, 3(2), 322–332. https://doi.org/10.22237/jmasm/1098673740

Hull, J. V., Dokovna, L. B., Jacokes, Z. J., Torgerson, C. M., Irimia, A., & Van Horn, J. D. (2017). Resting-state functional connectivity in autism spectrum disorders: A review. Frontiers in Psychiatry, 7, 205. https://doi.org/10.3389/fpsyt.2016.00205

Jia H, Yu D. Aberrant intrinsic brain activity in patients with autism spectrum disorder: insights from EEG microstates. Brain Topogr. (2019) 32:295–303. doi:10.1007/s10548-018-0685-0

Kalburgi, S. N., Bodfish, J. W., & Key, A. P. (2023). EEG microstates in autism spectrum disorder: A systematic review and meta-analysis. Neuroscience & Biobehavioral Reviews, 149, 105149. https://doi.org/10.1016/j.neubiorev.2023.105149

Khanna, A., Pascual-Leone, A., Michel, C. M., & Farzan, F. (2015). Microstates in resting-state EEG: Current status and future directions. Neuroscience & Biobehavioral Reviews, 49, 105–113. https://doi.org/10.1016/j.neubiorev.2014.12.010

Lehmann, D., Pascual-Marqui, R. D., & Michel, C. (2009). EEG microstates. Scholarpedia, 4(3), 7632. https://doi.org/10.4249/scholarpedia.7632

Menon, V. (2011). Large-scale brain networks and psychopathology: A unifying triple network model. Trends in Cognitive Sciences, 15(10), 483–506. https://doi.org/10.1016/j.tics.2011.08.003

Michalopoulos, K., Zervakis, M., Deiber, M. P., & Bourbakis, N. (2016). Classification of EEG single trial microstates using local global graphs and discrete hidden Markov models. International Journal of Neural Systems, 26(06), 1650036. https://doi.org/10.1142/S0129065716500368

Michel, C. M., & Koenig, T. (2018). EEG microstates as a tool for studying the temporal dynamics of whole-brain neuronal networks: A review. NeuroImage, 180, 577–593. https://doi.org/10.1016/j.neuroimage.2017.11.062

Milne, E. (2021). EEG data for "Electrophysiological signatures of brain aging in autism spectrum disorder". The University of Sheffield. Dataset. https://doi.org/10.15131/shef.data.16840351.v1

Milz, P., Faber, P. L., Lehmann, D., Koenig, T., Kochi, K., & Pascual-Marqui, R. D. (2016). The functional significance of EEG microstates—Associations with modalities of thinking. NeuroImage, 125, 643–656. https://doi.org/10.1016/j.neuroimage.2015.08.023

Nagabhushan Kalburgi, S., Kleinert, T., Aryan, D., Nash, K., Schiller, B., & Koenig, T. (2024). MICROSTATELAB: The EEGLAB toolbox for resting-state microstate analysis. Brain Topography, 37(4), 621–645. https://doi.org/10.1007/s10548-024-01034-9

Nagabhushan Kalburgi, S., Whitten, A. P., Key, A. P., & Bodfish, J. W. (2020). Children with autism produce a unique pattern of EEG microstates during an eyes closed resting-state condition. Frontiers in Human Neuroscience, 14, 288. https://doi.org/10.3389/fnhum.2020.00288

Nazary Sharif, H., Salar, S., & Haegele, J. A. (2023). The effect of training program on Autism Spectrum Quotient scores. Sport Sciences and Health Research, 15(2), 255-266. https://doi.org/10.22059/sshr.2024.328800.999

Neufeld, J., Soni, J., Engelhardt, C., Oathes, D. J., Nielson, D. M., & Tager-Flusberg, H. (2018). The neural basis of autism spectrum disorders: Structure, function, and connectivity. Neuroscience & Biobehavioral Reviews, 87, 70–82. https://doi.org/10.1016/j.neubiorev.2018.01.009

Pascual-Marqui, R. D., Lehmann, D., Faber, P., Milz, P., Kochi, K., Yoshimura, M., ... & Kinoshita, T. (2014). The resting microstate networks (RMN): Cortical distributions, dynamics, and frequency specific information flow. arXiv preprint arXiv:1411.1949.
Portnova, G., & Martynova, O. (2023, April 27). Macro- and microstates of resting-state EEG in children with low-functioning autism [Preprint]. Research Square. https://doi.org/10.21203/rs.3.rs-2844551/v1

Poulsen, A. T., Pedroni, A., Langer, N., & Hansen, L. K. (2018). Microstate EEGlab toolbox: An introductory guide. bioRxiv, 289850. https://doi.org/10.1101/289850

Quattrocki, E., & Friston, K. (2014). Autism, oxytocin and interoception. Neuroscience & Biobehavioral Reviews, 47, 410–430. https://doi.org/10.1016/j.neubiorev.2014.09.012

Ran, W., Wang, Y., Fang, H., Guan, L., Gao, J., Xu, X., Jin, H., & Ke, X. (2023). Distinct features of EEG microstates in autism spectrum disorder revealed by meta-analysis: The contribution of individual age to heterogeneity across studies. Frontiers in Psychiatry, 16, 1531694. https://doi.org/10.3389/fpsyt.2023.1531694

Romano, J., Kromrey, J. D., Coraggio, J., Skowronek, J., & Devine, L. (2006). Exploring methods for evaluating group differences on the NSSE and other surveys: Are the t-test and Cohen's d indices the most appropriate choices? In Annual meeting of the Southern Association for Institutional Research (pp. 1–51). https://files.eric.ed.gov/fulltext/ED529088.pdf

Seitzman, B. A., Abell, M., Bartley, S. C., Erickson, M. A., Bolbecker, A. R., & Hetrick, W. P. (2017). Cognitive manipulation of brain electric microstates. NeuroImage, 146, 533–543. https://doi.org/10.1016/j.neuroimage.2016.10.002

Takarae, Y., Zanesco, A., Keehn, B., Chukoskie, L., Müller, R. A., & Townsend, J. (2022). EEG microstates suggest atypical resting-state network activity in high-functioning children and adolescents with autism spectrum development. Developmental Science, 25(4), e13231. https://doi.org/10.1111/desc.13231

Tarailis, P., Koenig, T., Michel, C. M., & Griškova-Bulanova, I. (2024). The functional aspects of resting EEG microstates: a systematic review. Brain topography, 37(2), 181-217.

Tarailis, P., Šimkutė, D., Koenig, T., & Griškova-Bulanova, I. (2021). Relationship between spatiotemporal dynamics of the brain at rest and self-reported spontaneous thoughts: An EEG microstate approach. Journal of Personalized Medicine, 11(11), 1216. https://doi.org/10.3390/jpm11111216

Uddin, L. Q. (2015). Salience processing and insular cortical function and dysfunction. Nature Reviews Neuroscience, 16(1), 55–61. https://doi.org/10.1038/nrn3857

Uddin, L. Q., & Menon, V. (2009). The anterior insula in autism: Under-connected and under-examined. Neuroscience & Biobehavioral Reviews, 33(8), 1198–1203. https://doi.org/10.1016/j.neubiorev.2009.06.002

Uddin, L. Q., Supekar, K., Lynch, C. J., Khouzam, A., Phillips, J., Feinstein, C., Ryali, S., & Menon, V. (2013). Salience Network–Based Classification and Prediction of symptom severity in children with Autism. JAMA Psychiatry, 70(8), 869. https://doi.org/10.1001/jamapsychiatry.2013.104

Van de Ville, D., Britz, J., & Michel, C. M. (2010). EEG microstate sequences in healthy humans at rest reveal scale-free dynamics. Proceedings of the National Academy of Sciences, 107(42), 18179–18184. https://doi.org/10.1073/pnas.1007843107

Vargha, A., & Delaney, H. D. (2000). A critique and improvement of the CL common language effect size statistics of McGraw and Wong. Journal of Educational and Behavioral Statistics, 25(2), 101–132. https://doi.org/10.3102/10769986025002101

Wang, K., Li, K., & Niu, X. (2021). Altered functional connectivity in a Triple-Network model in autism with co-occurring attention deficit hyperactivity disorder. Frontiers in Psychiatry, 12. https://doi.org/10.3389/fpsyt.2021.736755

Wei, R., Wang, Y., Fang, H., Guan, L., Gao, J., Xu, X., Ke, X., & Jin, H. (2025). Distinct features of EEG microstates in autism spectrum disorder revealed by meta-analysis: The contribution of individual age to heterogeneity across studies. Frontiers in Psychiatry, 16, 1531694. https://doi.org/10.3389/fpsyt.2025.1531694

Yerys, B. E., Herrington, J. D., Satterthwaite, T. D., Guy, L., Schultz, R. T., & Bassett, D. S. (2019). Functional connectivity of fronto-parietal and salience/ventral attention networks have independent associations with co-occurring attention-deficit/hyperactivity disorder symptoms in children with autism. Biological Psychiatry: Cognitive Neuroscience and Neuroimaging, 4(4), 343–351. https://doi.org/10.1016/j.bpsc.2018.12.012

Yeshurun, Y., Nguyen, M., & Hasson, U. (2021). The default mode network: Where the idiosyncratic self meets the shared social world. Nature Reviews Neuroscience, 22(3), 181–192. https://doi.org/10.1038/s41583-020-00420-w

Zanesco, A. P., King, B. G., Skwara, A. C., & Saron, C. D. (2020). Within and between-person correlates of the temporal dynamics of resting EEG microstates. NeuroImage, 211, 116631. https://doi.org/10.1016/j.neuroimage.2020.116631

Highlights:

- EEG microstates reveal salience network instability in clinical ASD at rest
- TD-High ASQ individuals show intermediate neural traits, supporting a dimensional model of autistic traits.
- Microstate E shows heightened but brief engagement in ASD, indicating hyperarousal.
- Atypical sensory-to-salience transitions mark altered neural routing in ASD.